HHS Public Access

Author manuscript

Sci Transl Med. Author manuscript; available in PMC 2015 April 29.

Published in final edited form as:

Sci Transl Med. 2014 April 16; 6(232): 232ra50. doi:10.1126/scitranslmed.3008264.

Fibronectin^{EDA} Promotes Chronic Cutaneous Fibrosis Through Toll-like Receptor Signaling

Swati Bhattacharyya[1,*], **Zenshiro Tamaki**[1], **Wenxia Wang**[1], **Monique Hinchcliff**[1], **Paul Hoover**[2], **Spiro Getsios**[2], **Eric S. White**[3], and **John Varga**[1,*]

[1]Division of Rheumatology, Northwestern University Feinberg School of Medicine, Chicago, IL 60611, USA.

[2]Department of Dermatology, Northwestern University Feinberg School of Medicine, Chicago, IL 60611, USA.

[3]Department of Internal Medicine, University of Michigan, Ann Arbor, MI 48109–5642, USA.

Abstract

Scleroderma is a progressive autoimmune disease affecting multiple organs. Fibrosis, the hallmark of scleroderma, represents transformation of self-limited wound healing into a deregulated self-sustaining process. The factors responsible for maintaining persistent fibroblast activation in scleroderma and other conditions with chronic fibrosis are not well understood. Toll-like receptor 4 (TLR4) and its damage-associated endogenous ligands are implicated in immune and fibrotic responses. We now show that fibronectin extra domain A (Fn^{EDA}) is an endogenous TLR4 ligand markedly elevated in the circulation and lesional skin biopsies from patients with scleroderma, as well as in mice with experimentally induced cutaneous fibrosis. Synthesis of Fn^{EDA} was preferentially stimulated by transforming growth factor–β in normal fibroblasts and was constitutively up-regulated in scleroderma fibroblasts. Exogenous Fn^{EDA} was a potent stimulus for collagen production, myofibroblast differentiation, and wound healing in vitro and increased the mechanical stiffness of human organotypic skin equivalents. Each of these profibrotic Fn^{EDA} responses was abrogated by genetic, RNA interference, or pharmacological disruption of TLR4 signaling. Moreover, either genetic loss of Fn^{EDA} or TLR4 blockade using a small molecule

*Corresponding author. s-bhattacharyya@northwestern.edu (S.B.); j-varga@northwestern.edu (J.V.).

Author contributions: S.B. and J.V. conceived and designed the experiments. W.W., Z.T., S.B., and P.H. performed the experiments. S.B. and Z.T. analyzed the data. E.S.W., S.G., and M.H. contributed reagents/materials/analysis tools. S.B. and J.V. prepared the manuscript.

SUPPLEMENTARY MATERIALS

www.sciencetranslationalmedicine.org/cgi/content/full/6/232/232ra50/DC1

Fig. S1. Fn^{EDA} expression is elevated in bleomycin-treated mice.

Fig. S2. Attenuated Smad2 activation and elastin accumulation in Fn^{EDA}-null mice.

Fig. S3. Fn^{EDA} elicits TLR4-dependent proinflammatory and fibrotic responses.

Fig. S4. miR29 mediates fibroblast responses elicited by Fn^{EDA}.

Table S1. Primers for real-time qPCR.

Table S2. Comparison of patients with low versus high serum levels of Fn^{EDA}.

Citation: S. Bhattacharyya, Z. Tamaki, W. Wang, M. Hinchcliff, P. Hoover, S. Getsios, E. S. White, J. Varga, Fibronectin^{EDA} promotes chronic cutaneous fibrosis through Toll-like receptor signaling. Sci. Transl. Med. 6, 232ra50 (2014).

Competing interests: The authors declare that they have no competing interests.

mitigated experimentally induced cutaneous fibrosis in mice. These observations implicate the Fn^{EDA}-TLR4 axis in cutaneous fibrosis and suggest a paradigm in which aberrant Fn^{EDA} accumulation in the fibrotic milieu drives sustained fibroblast activation via TLR4. This model explains how a damage-associated endogenous TLR4 ligand might contribute to converting self-limited tissue repair responses into intractable fibrogenesis in chronic conditions such as scleroderma. Disrupting sustained TLR4 signaling therefore represents a potential strategy for the treatment of fibrosis in scleroderma.

INTRODUCTION

Scleroderma is a chronic disease of unknown etiology and substantial mortality characterized by autoimmunity, inflammation, and intractable tissue fibrosis. Because it has no validated biomarkers or effective disease-modifying therapies, scleroderma represents a major unmet medical need (1). The early inflammatory stage of scleroderma is often followed by tissue deposition of collagen-rich scar that disrupts the normal architecture and leads to dysfunction and eventual failure of the skin, lungs, and other organs (2). Although transforming growth factor–β (TGF-β) is recognized as an important trigger for fibroblast activation (3), the factors responsible for maintaining chronic fibrosis remain incompletely understood (4). As the primary extra-cellular matrix (ECM)–producing stromal cells, myofibroblasts serve as the key effectors of fibrogenesis (5). Multiple extracellular cues including soluble cytokines and chemokines, reactive oxygen species, and biomechanical signals induce stimulation of collagen and ECM molecule synthesis, and acquisition of a contractile myofibroblast phenotype. Ultimately, the establishment of self-amplifying feed-forward loops in lesional tissues may account for the failure to restrain fibro-blast activation, and a fundamental unanswered question in scleroderma is the nature of the autocrine and paracrine signaling pathways that underlie these loops (6).

Toll-like receptors (TLR) recognize both microbial pathogen-associated molecular patterns and nonmicrobial endogenous ligands (7). Endogenous TLR4 ligands display molecular patterns that are normally inaccessible to the immune system but are released passively into the extracellular space upon cell injury or necrosis, or activation after chronic injury. Matrix molecules such as biglycan, tenascin C, and hyaluronic acid are up-regulated or undergo oxidation or fragmentation upon tissue injury and serve as potential endogenous TLR4 ligands (8). Because they are normally inert and are recognized by TLRs only upon injury, these “damage-associated molecular patterns” (DAMPs) serve as danger signals that enable the innate immune system to sense and respond to sterile tissue damage (9, 10). Accumulating evidence implicates DAMP-triggered aberrant TLR signaling in chronic inflammatory and fibrotic disorders, as well as in mouse models of disease (11–14). Skin and lung biopsies from patients with scleroderma show elevated levels of endogenous TLR4 ligands and constitutive TLR4 signaling, but the signals responsible for TLR4 activation and their role in pathogenesis remain unknown (15, 16).

Fibronectins are high–molecular weight modular glycoproteins that circulate in soluble form in plasma or accumulate in tissue as insoluble ECM components (17). Because of alternate splicing of the fibronectin gene, cellular fibronectin contains extra domains A (EDA) and B

(EDB), which are excluded from plasma fibronectin (18). The EDA-containing fibronectin variant (Fn^{EDA}) fulfills dual function as both structural ECM scaffold and signaling molecule regulating adhesive, proliferative, and migratory cellular responses, and plays an important role in myofibroblast differentiation and wound healing (19, 20). Although there is little Fn^{EDA} expression in adult tissues, marked transient up-regulation is seen during normal wound healing and tissue repair (21–24). Cellular responses elicited by Fn^{EDA} are mediated via both surface integrins and TLR4 (24–28).

The present studies were undertaken to investigate the expression and regulation of Fn^{EDA} in scleroderma, and its role and mechanism of action in fibrosis. The results reveal significant elevation of Fn^{EDA} in the serum and skin from patients with scleroderma, as well as in lesional tissues from mice with cutaneous fibrosis. Exogenous Fn^{EDA} had potent effects on collagen gene expression, myofibroblast differentiation and in vitro wound healing, and increased matrix stiffness and collagen cross-linking in human skin equivalents. These ex vivo fibrotic responses were abolished by either genetic or pharmacological disruption of fibroblast TLR4 signaling. Moreover, mice lacking Fn^{EDA} or treated with a TLR4 inhibitor showed attenuation of inducible cutaneous fibrosis. Together, our results indicate that Fn^{EDA} is aberrantly expressed in patients with scleroderma, induces fibrotic response via TLR4, and is required for maximal cutaneous fibrogenesis in the mouse. On the basis of these findings, we propose the following paradigm for pathological fibrogenesis: Injury triggers increased production and persistent extracellular accumulation of Fn^{EDA}, which in turn induces TLR4-dependent fibrotic responses including Fn^{EDA} synthesis. The ensuing positive feedback loop is likely to contribute to the persistence and progression of fibrosis in scleroderma. The results from these studies might inform the development of therapeutic approaches to control fibrosis in scleroderma.

RESULTS

Elevated Fn^{EDA} levels in scleroderma

To assess Fn^{EDA} expression in scleroderma, we pursued two approaches. First, serum levels were determined in 48 patients with diffuse cutaneous scleroderma and 16 healthy adults recruited from a single institution. The clinical characteristics of the subjects are shown in Table 1. Ninety-five percent of the scleroderma patients were women, and 18 had early-stage (<2 years) disease. A fivefold increase in serum Fn^{EDA} levels was seen in scleroderma patients compared to control subjects (mean, 20.2 ± 1.6 μg/ml versus 4.5 ± 0.8 μg/ml; $P < 0.0001$) (Fig. 1A). The 95% confidence interval in control subjects was <6.3 μg/ml; 94% of scleroderma patients had elevated Fn^{EDA} levels. No significant correlation was found between Fn^{EDA} levels and disease duration, modified Rodnan skin score (mRSS), forced vital capacity (FVC) or diffusing capacity for carbon monoxide (DLco), or change in mRSS during a 6-month follow-up period (tables S1 and S2).

Next, tissue levels of Fn^{EDA} mRNA and protein were examined. RNA was isolated from biopsies of lesional skin from 20 scleroderma patients or forearms of 8 healthy volunteers (Table 2). Real-time quantitative polymerase chain reaction (qPCR) results showed a nearly threefold increase ($P = 0.0002$) in Fn^{EDA} mRNA in scleroderma biopsies compared to matched controls (Fig. 1B). Immunofluorescence showed that healthy control skin ($n = 6$)

had only barely detectable Fn^{EDA} in the dermis, whereas scleroderma biopsies ($n = 13$) displayed a more than twofold increase ($P = 0.016$) (Fig. 1C and Table 3). Together, these results indicate that the Fn^{EDA} splice variant is selectively elevated in both serum and lesional skin biopsies from patients with scleroderma.

Preferential stimulation of Fn^{EDA} in TGF-β–treated normal fibroblasts

The elevated expression of Fn^{EDA} in scleroderma patients prompted us to investigate the mechanisms underlying its regulation. For this purpose, quiescent foreskin fibroblasts were incubated with TGF-β for up to 48 hours, and RNA and protein were analyzed by real-time qPCR and immunoblotting. The results showed that TGF-β induced a dose-dependent increase in levels of both Fn^{EDA} mRNA (maximal >30-fold) and protein (>9-fold) in these fibroblasts (Fig. 1D). In contrast to the marked up-regulation of the EDA splice variant, fibronectin showed only a modest (about threefold) increase in response to TGF-β. To identify signaling pathways underlying TGF-β stimulation of Fn^{EDA}, fibroblasts were pretreated with the selective activin receptor-like kinase 5 (ALK5) inhibitor SB431542 or the mitogen-activated protein kinase kinase (MEK1/2) inhibitor U0126 for 30 min before the addition of TGF-β. The stimulatory effects of TGF-β on Fn^{EDA} were completely abolished in the presence of SB431542, whereas U0126 had no effect, indicating a primary role for the canonical Smad pathway (Fig. 1E).

Attenuated dermal fibrosis in Fn^{EDA}-null mice

To explore the potential role of Fn^{EDA} in tissue remodeling in vivo, mice with homozygous exclusion of the EDA were studied (21). Fn^{EDA}-null mice were viable, developed normally, and showed no overt pheno-type. Cutaneous fibrosis was induced by daily subcutaneous injections of bleomycin (15). Mice were sacrificed at day 24, and lesional skin was harvested for analysis. A twofold increase in dermal thickness ($P < 0.0001$) and collagen accumulation ($P = 0.02$) was evident in wild-type C57BL/6 mice treated with bleomycin (Fig. 2A). Similarly treated Fn^{EDA}-null mice showed significantly reduced dermal thickness ($P < 0.001$) and collagen ($P = 0.015$). Immunofluorescence demonstrated a marked increase in Fn^{EDA} accumulation in the dermis in wild-type mice injected with bleomycin, whereas no Fn^{EDA} could be detected in Fn^{EDA}-null mice, as expected (fig. S1, A and B). Real-time qPCR results showed that bleomycin-induced up-regulation of collagen and α smooth muscle actin (αSMA) mRNA in the fibrotic skin was significantly attenuated, and the proportion of αSMA-positive fibroblasts markedly decreased, in Fn^{EDA}-null mice (Fig. 2, B and C). Moreover, the increase in the number of phospho-Smad2–positive cells in the fibrotic dermis was significantly attenuated in Fn^{EDA}-null mice (fig. S2, A and B).

Multiple ECM components are implicated in the progression of organ fibrosis (29). Elastin, the main component of elastic fibers, provides structural integrity and is responsible for the elastic properties of the skin and other organs (30, 31). Previous studies have implicated aberrant elastin deposition and organization in scleroderma, as well as murine models of fibrosis (32–34). To examine the role of Fn^{EDA} in elastic fiber accumulation, we examined lesional skin from wild-type and Fn^{EDA}-null mice by Verhoeff–Van Gieson staining. In wild-type mice, short wavy stretches of elastic fibers were seen throughout the dermis scattered randomly between adjacent collagen fibers (fig. S2, C and D). Development of

dermal fibrosis was accompanied by an increase in the number of elastic fibers, and of elongated fibers, in wild-type mice, but not in Fn^{EDA}-null mice.

To further evaluate the role of Fn^{EDA}, we induced cutaneous fibrosis in wild-type and Fn^{EDA}-null mice in parallel by subcutaneous injections of adenovirus expressing constitutively active TGF-β1 (AdTGF-β1). Mice were sacrificed 28 days after the second subcutaneous injection, and lesional skin was analyzed. In contrast to wild-type mice that showed a ~50% increase in dermal thickness ($P = 0.02$), in Fn^{EDA}-null mice, AdTGF-β1 elicited only a 15% increase ($P = 0.20$) (Fig. 2D). Moreover, collagen fiber deposition in the lesional dermis was notably attenuated. Results from these complementary animal models together indicate that Fn^{EDA} plays a fundamental role in the development of experimentally induced cutaneous fibrosis.

Stimulation of collagen synthesis and myofibroblast differentiation by Fn^{EDA}

To investigate the regulation of fibrotic responses by Fn^{EDA}, we seeded normal dermal fibroblasts in plastic dishes, and confluent mono-layers were incubated with Fn^{EDA} (5 or 10 μg/ml) for up to 72 hours. Real-time qPCR and Western analysis demonstrated a dose-dependent increase in COL1A1 mRNA expression and type I collagen levels (Fig. 3A). Comparable stimulation of collagen gene expression was noted in scleroderma skin fibroblasts stimulated with Fn^{EDA} (fig. S3A). Furthermore, treatment with Fn^{EDA} resulted in substantially enhanced αSMA expression and stress fiber incorporation (Fig. 3B). In stark contrast to Fn^{EDA}, fibronectin had no effect on collagen and αSMA expression under similar experimental conditions (fig. S3E). Furthermore, preincubation of the cultures with a neutralizing antibody specific for the EDA domain abrogated the profibrotic effects, indicating the essential role of the EDA domain in triggering these responses (fig. S3E).

Cell migration and matrix contraction are fibroblast responses required for effective wound healing, and their deregulation is implicated in pathological fibrogenesis (35, 36). To evaluate the effect of Fn^{EDA} on in vitro wound healing, we used a pipette tip to create a linear scratch in confluent fibroblast monolayers plated on dishes coated with or without Fn^{EDA} (10 μg/ml), and cell migration into the wounded area was monitored for up to 48 hours. As shown in Fig. 3C (left panel), fibroblasts grown on Fn^{EDA}-coated plastic showed significantly accelerated migration compared to fibroblasts on uncoated plastic. Moreover, fibroblast contractility in collagen gels was enhanced when Fn^{EDA} (10 μg/ml) was incorporated in the gels (Fig. 3C, right panel).

Substrate stiffness has profound influence on fibrogenesis by modulating fibroblast morphology, migration, differentiation, and survival (37). Plastic dishes traditionally used for cell culture studies present an excessively rigid substrate with stiffness approaching 2 GPa, potentially confounding the interpretation of the results (38). To dissociate the effect of Fn^{EDA} on fibroblasts from that of mechanical forces imparted by the stiff substrate, we took an alternate experimental approach using human fibroblasts embedded in three-dimensional (3D) organotypic skin raft cultures that spontaneously organize a “dermal compartment” with mechanical stiffness approximating that of normal dermis (39). Normal fibroblasts were embedded in skin rafts made with or without Fn^{EDA} for 14 days, followed by harvesting and analysis of the dermal compartment. Inclusion of Fn^{EDA} in the rafts was

associated with a significant increase in deposition of cross-linked “mature” collagen (Fig. 3D). Western analysis confirmed increased collagen (1.8-fold) and αSMA (~1.7-fold) accumulation in the dermal compartment when Fn^{EDA} was included (Fig. 3E). We next examined the effect of Fn^{EDA} on substrate stiffness in the 3D skin equivalents. Organotypic human skin equivalents constructed using collagen only elaborated a matrix that had physiological stiffness (~600 Pa), whereas incorporation of Fn^{EDA} into the rafts resulted in a concentration-dependent increase in stiffness of the dermal compartment (Fig. 3F). Stiff substrates directly promote fibrogenesis by eliciting fibrotic responses such as type I collagen production in explanted fibroblasts (37, 39). These complementary ex vivo models together demonstrate that Fn^{EDA} exerts potent profibrotic effect on fibroblasts in both 2D monolayers and 3D skin organotypic human skin equivalents.

Fn^{EDA}, an endogenous TLR4 ligand

In murine mast cells and macrophages, Fn^{EDA} binds to and activates TLR4 (25, 26). Whole-cell lysates from fibroblasts incubated with or without TGF-β for 24 hours were immunoprecipitated sequentially with TLR4, Fn^{EDA}, or control immunoglobulin G (IgG) and immuno-blotted with antibodies to TLR4 or Fn^{EDA} to examine whether Fn^{EDA} functions as a TLR4 ligand in skin fibroblasts. The results revealed direct interaction of cellular TLR4 with Fn^{EDA} in unstimulated fibro-blasts, which was increased in TGF-β–treated fibroblasts (Fig. 4A).

To evaluate how Fn^{EDA} modulates TLR4 signaling in fibroblasts, we first examined TLR4-dependent inflammatory responses. A series of experiments demonstrated that incubation of fibroblasts with Fn^{EDA} elicited a range of classic inflammatory TLR4 responses, including marked stimulation of interleukin-6 (IL-6) secretion and NF-κB-luc activity (Fig. 4B and fig. S3). The stimulatory effect of Fn^{EDA} was attenuated when cultures were pretreated with neutralizing antibodies specific for the EDA domain (Fig. 4B). Furthermore, the stimulatory effects of Fn^{EDA} were unaffected by pretreatment with polymyxin B in contrast to lipopolysaccharide (LPS), excluding a role for potential endotoxin contamination of the Fn^{EDA} preparations (fig. S3C).

Fn^{EDA}-mediated fibrotic responses via TLR4

Having demonstrated a direct interaction of Fn^{EDA} with TLR4 in fibroblasts, three complementary loss-of-function approaches were pursued to assess the role of TLR4 in mediating the profibrotic effect of Fn^{EDA}. First, we showed that pretreatment of fibroblasts with CLI-095, a small molecule that selectively blocks TLR4 responses by binding to its intracellular signaling domain (40), completely abrogated Fn^{EDA}-induced stimulation of type I collagen accumulation and αSMA synthesis (Fig. 4C). Second, selective small interfering RNA (siRNA) knockdown of TLR4 was accompanied by substantially reduced Fn^{EDA} stimulation of collagen gene expression and myofibroblast differentiation (Fig. 4D). To further confirm the essential role of TLR4 in the Fn^{EDA} response, we pursued a genetic loss-of-function approach using TLR4-mutant C3H/HeJ mice that harbor a TLR4 missense mutation, resulting in LPS hyporesponsiveness (41). Primary skin fibroblasts ex-planted from C3H/HeJ mice and wild-type C3H/HeOuJ mice were grown to confluence in parallel and incubated with Fn^{EDA} for 72 hours. Western analysis showed that in contrast to wild-

type control fibro-blasts, in TLR4-mutant fibroblasts, Fn^{EDA} failed to stimulate collagen synthesis (Fig. 4E). Endotoxin contamination could not account for the stimulatory responses because preincubation of the cultures with polymyxin B did not abrogate the profibrotic effect of Fn^{EDA} while effectively blocking LPS-induced cytokine as well as COL1A1 induction (fig. S3D). Moreover, stripping the Fn^{EDA} preparation of LPS also failed to abrogate the stimulatory effects (Fig. 4B and fig. S3F). Together, these pharmacological, RNA interference, and genetic approaches in combination unequivocally establish the sufficient and necessary role for TLR4 in mediating profibrotic responses elicited by Fn^{EDA}.

To gain insight into the cellular mechanisms underlying the TLR4-dependent profibrotic Fn^{EDA} responses, we examined the potential role of miR29, a microRNA of particular interest in light of its emerging role as master regulator of fibrotic responses implicated in scleroderma (15, 42, 43). Incubation of normal fibroblasts with Fn^{EDA} caused suppression of miR29a and miR29b, with a maximal ~60% decrease at 72 hours (fig. S4A). The inhibitory response was abrogated by CLI-095, indicating its dependence on TLR4 (fig. S4B). Significantly, pre-miR29a abrogated the collagen stimulatory effect of Fn^{EDA}, whereas miR29-specific antagomirs caused an increase in basal levels of COL1A1 mRNA and further enhanced the stimulatory response elicited by Fn^{EDA} (fig. S4, C and D). These observations suggest that down-regulation of miR29 might be a mechanism underlying the profibrotic responses elicited by Fn^{EDA}.

Essential role of TLR4 for the development of cutaneous fibrosis

Because our in vitro studies implicated Fn^{EDA}-TLR4 signaling in fibrosis, we sought to evaluate the pathogenetic role of TLR4 in vivo using pharmacological TLR4 inhibition. Mice were given daily injections of sub-cutaneous bleomycin alone or concurrently with the TLR4 inhibitor CLI-095. There was no weight loss or other evidence of toxicity in mice treated with CLI-095. Lesional skin from mice treated with bleomycin showed a substantial increase in dermal thickness, accumulation of densely packed collagen bundles accompanied by loss of subcutaneous adipose, and marked necrosis of the subjacent skeletal muscle (Fig. 5A). Mice treated with CLI-095 showed a significantly attenuated increase in dermal thickness ($P < 0.001$) and collagen deposition (24.0 to 11.4%, $P = 0.034$). Moreover, bleomycin-induced muscle necrosis was virtually absent. Real-time qPCR showed that CLI-095 treatment mitigated the up-regulation of COL1A1 and αSMA mRNA in the skin (Fig. 5B). Additional experiments showed that TLR4 blockade reversed cutaneous fibrosis, with reduced dermal thickness, collagen accumulation (18.6 to 11.4%, $P = 0.011$), and collagen and αSMA mRNA expression, when mice were treated with CLI-095 starting at day 15 (Fig. 5, C and D). These results demonstrate that pharmacological blockade of TLR4 using a well-tolerated small molecule both prevented and promoted regression of skin fibrosis, suggesting an essential role for TLR4 signaling in its development and persistence.

DISCUSSION

In scleroderma, the tightly regulated and self-limited repair process that normally leads to tissue regeneration in the skin and multiple organs is subverted, and the ensuing persistent

fibroblast activation underlies pathological fibrosis (6, 11–14). We now show that an alternately spliced variant of fibronectin that is normally absent in adult tissue but up-regulated transiently upon injury was constitutively raised in both the serum and skin biopsies from patients with scleroderma, and its expression in normal fibroblasts was stimulated preferentially by TGF-β. Serving as a bona fide endogenous TLR4 ligand, Fn^{EDA} elicited potent TLR-dependent fi brotic responses in monolayer fibroblast cultures and in organotypic human skin equivalents. Moreover, in mice, both genetic deletion of Fn^{EDA} and pharmacologic blockade of TLR4 mitigated cutaneous fibrosis. Together, these observations identify an Fn^{EDA}-TLR4 axis as a pathway fundamental for maintaining sustained fibroblast activation implicated in scleroderma.

The Fn^{EDA} splice variant is prominently expressed in embryogenesis but becomes undetectable in adults (17). Physiologic tissue remodeling is associated with transient expression of Fn^{EDA}, whereas cancer and chronic inflammation are associated with sustained elevation (44–49). Circulating levels of Fn^{EDA} show marked increase after trauma, stroke, and ischemic heart disease (20), and elevated circulating Fn^{EDA} predicts liver fibrosis in patients with chronic hepatitis C patients (50). We found elevated Fn^{EDA} levels in the serum as well as in skin biopsies from patients with scleroderma. Previous studies demonstrated aberrant Fn^{EDA} deposition in scleroderma lesional skin (51), and in lungs from patients with idiopathic pulmonary fibrosis (24), suggesting persistent tissue accumulation of Fn^{EDA} as a hallmark of fibrosis. Autocrine TGF-β signaling is thought to underlie the constitutively activated fibroblast phenotype in scleroderma (52). We found that in normal fibroblasts, TGF-β caused a marked stimulation of Fn^{EDA}, but only modest change in total fibronectin, a selective response consistent with previous reports (53, 54). Another splice variant of fibronectin, Fn^{EDB}, was undetected in scleroderma skin biopsies. We speculate that autocrine TGF-β stimula-tory loops in the scleroderma lesion underlie the persistence of Fn^{EDA} expression, but the mechanisms regulating alternative splicing of fibronectin in scleroderma fibro-blasts remain to be uncovered.

Myofibroblast differentiation is an essential step in the formation of fibrosis, and Fn^{EDA} is indispensable for the process (19). Our results demonstrate that in ex-planted skin fibroblasts in monolayers and fibroblasts embedded in 3D organotypic human skin equivalents, Fn^{EDA} elicited a range of fibrotic responses (39). Previous studies indicated that recombinant Fn^{EDA} interacts with and signals through TLR4 (25, 26, 28). Our present results confirm that Fn^{EDA} is an endogenous TLR4 ligand in skin fibroblasts. It has been shown that unfolding of Fn^{EDA} caused by tensional forces in the fibrotic microenvironment exposes the EDA domain (55). Thus, in the stiff scleroderma skin, TGF-β–driven Fn^{EDA} synthesis, combined with exposure of its EDA domain caused by unfolding due to rigid matrix, is likely to increase Fn^{EDA} bioavailability as an endogenous TLR4 ligands. The present results indicate that in addition to signaling via $\alpha_4\beta_1$, $\alpha_4\beta_7$, and $\alpha_9\beta_1$ integrins (56–59), Fn^{EDA} also uses TLR4 to elicit cellular responses.

A fundamental role of Fn^{EDA} in fibrosis is underscored by our results showing that Fn^{EDA}-null mice were protected from cutaneous fibrosis. Previous studies demonstrated aberrant wound healing and attenuated lung fibrosis in mice lacking Fn^{EDA} (21, 24, 55). Inhibition of TLR4 was shown to attenuate Fn^{EDA}-mediated ischemic brain injury, highlighting the

importance of the Fn^{EDA}-TLR4 axis in this context (60). We now show that pretreatment with a TLR4 inhibitor prevented cutaneous fibrosis, collagen deposition, and myofibroblast accumulation and caused regression of established fibrosis when given therapeutically. Micro-RNAs play fundamental roles in a variety of cellular responses. In particular, miR29 is thought to be important in controlling fibro-genesis and shows reduced expression in fibrotic conditions including scleroderma (61–64). In the present studies with normal fibroblasts, Fn^{EDA} suppressed miR29a expression in a TLR4-dependent manner. Rescuing miR29a expression in Fn^{EDA} -treated fibroblasts abrogated the stimulation of collagen gene expression, whereas suppressing miR29a using an antagomir enhanced the response, implicating miR29 as a possible mediator of the TLR4-driven profibrotic effects of Fn^{EDA} (42, 65).

There are limitations to the current study. The cohort evaluated for serum Fn^{EDA} levels was relatively small, precluding firm conclusions regarding the utility of serum Fn^{EDA} as a biomarker in scleroderma or as a marker of organ involvement or disease activity. It should be informative to compare serum Fn^{EDA} levels in chronic autoimmune and fibrotic diseases. Although our results demonstrate marked Fn^{EDA} accumulation in lesional skin, it remains to be determined whether it is Fn^{EDA} or other endogenous TLR4 ligands that are primarily responsible for maintaining the activated fibroblast phenotype in scleroderma lesions. Indeed, several such damage-associated endogenous TLR4 ligands have been shown to be elevated in scleroderma, including hyaluronan and biglycan. In addition, although the present results clearly implicate the Fn^{EDA}-TLR4 axis in cutaneous fibrosis induced by bleomycin or TGF-β, it will be of great interest to explore the pathogenetic role of the Fn^{EDA} TLR4 axis in other forms of cutaneous and extracutaneous organ fibrosis.

On the basis of our in vitro and in vivo observations, we propose a model for persistent cutaneous fibrosis (Fig. 5), where activated fibro-blasts exposed to extracellular Fn^{EDA} within the fibrotic milieu acquire a TLR4-dependent fibrotic phenotype with further stimulation of the production and deposition of ECM molecules including Fn^{EDA}, thereby exacerbating and sustaining fibrogenesis. In this way, fibroblast innate immune signaling triggered by DAMPs might represent one of the cellular pathways responsible for converting self-limited regenerative repair into an intractable fibrotic process. Accordingly, we propose that disrupting sustained TLR4 signaling in the skin lesion represents a potential strategy for breaking the vicious cycle of fibrosis in scleroderma.

MATERIALS AND METHODS

Study design

This was an observational study designed to identify differences among scleroderma patients and healthy controls. Serum levels of Fn^{EDA} were determined in 48 scleroderma patients evaluated at a single center and 16 healthy controls in parallel. All patients met American College of Rheumatology criteria for the classification of systemic sclerosis (SSc) (66) and were sub-classified as limited or diffuse cutaneous disease using published criteria (67). Duration of disease was defined as the interval from the onset of the first non-Raynaud disease manifestation to the time of the serum collection, and patients were subdivided into early (<24 months) and late (>24 months) subgroups. Pulmonary function testing was

performed within 6 months of the time of serum collection (68). To assess Fn^{EDA} accumulation in lesional tissue, skin biopsies from the clinically involved forearm of 13 SSc patients and 7 healthy controls were processed in parallel for immunofluorescence. RNA was isolated from skin biopsies of 19 scleroderma patients and 9 healthy controls and processed for real-time qPCR.

Animal experiments were performed according to institutionally approved protocols and in compliance with the guidelines of the Northwestern University Animal Care and Use Committee. In selected experiments, mice were randomly assigned to treatment groups, and treatment groups were blinded during experimental procedures and raw data analysis. No animals or potential outliers were excluded from the data sets presented in this study. All in vitro studies were performed in replicates (n = 3, unless otherwise specified).

Cell culture and reagents

Primary human fibroblast cultures were established by explantations from neonatal foreskin or from skin biopsies of the clinically affected forearms of patients with scleroderma and the forearm of healthy adult volunteers (15). Biopsies were performed with written informed consent and in accordance with protocols approved by the Institutional Review Board for Human Studies at Northwestern University. Primary fibroblasts at low passage grown in monolayers in plastic dishes were studied at early confluence or were embedded into “dermal” collagen plugs used to create 3D organotypic human skin equivalents (15, 69, 70). Skin fibroblast cultures were also established from 8-week-old C3H/HeJ (TLR4-mutant) and C3H/HeOuJ (wild-type) mice (The Jackson Laboratory) and studied in parallel. Cultures were maintained in Dulbecco's modified Eagle's medium (DMEM) supplemented with 10% fetal calf serum (Gibco BRL), 1% vitamin solutions, and 2 mM L-glutamine. All other tissue culture re-agents were from Lonza. Cultures were placed in serum-free medium containing 0.1% bovine serum albumin (BSA) for 24 hours before addition of TGF-β (PeproTech) or Fn^{EDA}. To generate Fn^{EDA}, conditioned media were collected from human embryonic IMR90 fibroblasts incubated for 48 hours and purified with affinity chromatography (24). The purity of Fn^{EDA} was confirmed by Coomassie staining and by Western analysis (fig. S3A, left panel)). Endotoxin was quantitated in the Fn^{EDA} preparations with Pierce LAL Chromogenic Endotoxin Quantitation Kit (Thermo Fisher Scientific). In selected experiments, cultures were incubated in medium with Fn^{EDA} preparations that had been subjected to endotoxin removal with Pierce High Capacity Endotoxin Removal Resin (Thermo Fisher Scientific). The TLR4 inhibitor CLI-095 (InvivoGen) or neutralizing antibodies specific for the EDA domain (IST9, Abcam) were added to the cultures 60 min before Fn^{EDA}. Levels of IL-6 secreted in the medium were determined by ELISA (R&D Systems).

Fn^{EDA} effects in 3D organotypic human skin equivalents

To evaluate the effects of Fn^{EDA} in 3D organotypic human skin equivalents, foreskin fibroblasts (300,000 cells/ml) were resuspended in rat tail type I collagen (4 mg/ml, from BD Biosciences) with or without Fn^{EDA} (10 μg/ml) and seeded in 12-well plates (69). Briefly, foreskin fibroblasts (300,000 cells/ml) were resuspended in a buffered solution of rat tail type I collagen (4 mg/ml, from BD Biosciences) with or without Fn^{EDA} (10 μg/ml)

and seeded in 12-well cell culture plates (1.5 ml per well). The dermal collagen plugs were allowed to polymerize for 30 min and then supplemented with 10% DMEM overnight. Primary human epidermal keratinocytes (200,000 cells/ml) isolated from a pool (n = 3) of neonatal foreskins were seeded on top of the dermal collagen plug in E medium [3:1 of DMEM/Ham's F-12 containing 180 μM adenine, insulin (5 μg/ml), transferrin (5 μg/ml), T3 (5 μg/ml), hydrocortisone (0.4 ng/ml), and cholera toxin (10 mg/ml)] supplemented with epidermal growth factor (5 ng/ml) as previously described (70). After 48 hours of incubation, the skin equivalents were transferred to the top of a metal grid raised above the surface of a 60-mm tissue culture dish and exposed to air to promote epidermal stratification. Culture media were replaced every other day for up to 12 days, and rafts were harvested and lysed for Western analysis, fixed in 10% neutral buffered formalin, and embedded in paraffin for staining or processed for determination of stiffness. Picrosirius Red staining was used to evaluate collagen deposition and fiber alignment in the dermal compartment.

To determine the effect of Fn^{EDA} on substrate stiffness in organotypic raft cultures, a parallel-plate rheometer (Oscillatory Shear Paar Physica MCR Rheometer, Anton Paar GmbH) was used. Circular samples (20-mm diameter) of control and Fn^{EDA}-containing rafts were placed between parallel plates, and plate distance of 0.2 mm was preset to compress the raft. Frequency (F = 0.1 to 10 Hz) sweep tests under oscillatory conditions were conducted at a constant temperature of 37°C, with controlled shear deformation $\gamma = 0.5\%$ and 15 measuring points, which led to an average test duration of 16 min. Results, expressed as Young's modulus, were calculated with US-200 software (Anton Paar Co.).

In vitro cell migration and collagen gel contraction assays

The effects of Fn^{EDA} on modulating fibroblast function were further evaluated by in vitro wound healing and collagen gel contraction assays (36). Briefly, human skin fibroblasts were seeded on Fn^{EDA}-coated plates, and confluent monolayers in serum-free DMEM were mechanically wounded with standard p1000 pipette tips. Cultures were monitored for up to 48 hours by phase-contrast microscopy, and pictures were taken at ×25 magnification. The wound gap width (micrometers) was determined at six randomly selected sites per slide at indicated intervals. Collagen gel contraction assays were performed with fibro-blasts seeded in type I collagen gels as described (36). After incubation of the gels in medium containing Fn^{EDA} (10 μg/ml) for the indicated intervals, gel diameters were determined with ImageJ software [National Institutes of Health (NIH), Bethesda, MD]. All experiments were performed in triplicate.

Isolation and analysis of RNA and microRNA

At the end of the experiments, total RNA was isolated from explanted fibroblasts, skin biopsies, or organotypic skin rafts and reverse-transcribed to complementary DNA (cDNA) with SuperMix as described (cDNA Synthesis SuperMix, Quanta BioSciences) (15). The products (50 ng) were amplified with SYBR Green PCR Master Mix (Applied Biosystems) on an Applied Biosystems 7500 Prism Sequence Detection System. The sequence of the primers is shown in Table 1. MicroRNA was isolated from confluent fibroblasts with the mirVana miRNA Isolation Kit (Ambion/Applied Biosystems) and amplified with TaqMan

probes (Applied Biosystems). Levels of miRNA were determined by qPCR with Applied Biosystems 7500 Prism Sequence Detection System (15). Data were normalized to GAPDH RNA, and fold change in samples was calculated as $2^{-\Delta\Delta Ct}$ {2−[(Ct target − Ct GAPDH) treatment − (Ct target − Ct GAPDH) nontreatment]}.

Western and immunoprecipitation/immunoblot analysis

At the end of the experiments, fibroblasts were harvested, whole-cell lysates were prepared, and equal amounts of proteins (20 to 50 μg per lane) were subjected to Western analysis with primary antibodies specific for type I collagen (Southern Biotechnology), Fn^{EDA} (Sigma-Aldrich), and tubulin (Sigma-Aldrich) as described (15). Membranes were then incubated with appropriate secondary antibodies and subjected to enhanced chemiluminescence detection with ECL Reagent (Pierce). In other experiments, whole-cell lysates (~600 μg) were immunoprecipitated and subjected to immunoblot analysis with antibodies to Fn^{EDA} (Sigma-Aldrich) and TLR4 (Santa Cruz Biotechnology). Band intensities were quantitated with ImageJ software and corrected for tubulin in each lane.

Transient transfection assays

Subconfluent skin fibroblasts in serum-free medium were transfected with NF-κB-luc with SuperFect reagent (Qiagen), followed by incubation in medium containing Fn^{EDA} (10 μg/ml) in the presence or absence of neutralizing EDA domain–specific antibodies (IST9) and polymyxin B for 24 hours. Cultures were harvested, and whole-cell ly-sates were assayed for their luciferase activities. In each experiment, fibroblasts were cotransfected with *Renilla* luciferase pRL-TK plasmids (Promega) as controls for transfection efficiency. Experiments were performed in triplicate and repeated at least twice with consistent results.

Immunofluorescence confocal microscopy

To assess the modulation of fibroblast responses by Fn^{EDA} by immunocytochemistry, fibroblasts on eight-well Lab-Tek II chamber glass slides (Nalgene Nunc International) were incubated in serum-free DMEM supplemented with 0.1% BSA containing Fn^{EDA} (10 μg/ml) for up to 72 hours. In selected experiments, fibroblasts were transfected with TLR4-specific siRNA or scrambled control siRNA (Dharmacon) for 24 hours before the addition of Fn-EDA. Cells were then fixed, permeabilized, and incubated with antibodies to type I collagen or αSMA (Sigma) at 1:100 or 1:500 dilution, followed by Alexa Fluor– labeled secondary antibodies (Invitrogen). Nuclei were identified with DAPI. Subcellular distribution of immunofluorescence was evaluated under an immunofluorescence microscope or Zeiss UV Meta 510 confocal microscope (Carl Zeiss Inc.) (15).

Serum Fn^{EDA} determinations by ELISAs

To determine serum levels of Fn^{EDA}, we developed a specific ELISA. Briefly, 96-well plates were coated with primary antibody to Fn^{EDA} (3E2, Sigma) (1.4 μg/ml in 0.05 M carbonate-bicarbonate buffer, pH 9.6) for 60 min at 37°C followed by blocking with 5% BSA. Serum samples in triplicate were incubated with peroxidase-conjugated goat anti-human fibronectin IgG (1:8000; MP Biomedicals, LLC; catalog no. 55240) for 30 min and washed four times with PBS. Substrate solution (50 μl) was added, and after sufficient color

development, reactions were terminated with 0.5 M sulfuric acid and absorbance at 490 nm was measured with an automated plate reader. The sample concentrations were interpolated from standard curves prepared with serial dilutions of known Fn^{EDA} concentrations (detection range, 0.8 to 50.0 μg/ml). To ensure specificity, all assays were run with plasma fibronectin as a negative control.

Fn^{EDA} expression in scleroderma skin biopsies

Paraffin-embedded sections (4 μm) were incubated with primary antibodies against Fn^{EDA} (Sigma, 1:50), followed by mouse Alexa Fluor secondary antibodies (Invitrogen) or DAPI. Slides were mounted, and immunofluorescence was evaluated under a Zeiss UV Meta 510 confocal microscope. Immunopositivity was specific for Fn^{EDA} because substitution of the primary antibody resulted in the absence of staining and Western blot using the antibody showed a single band. Computer-generated 3D image plots of fluorescence intensity were analyzed with ImageJ software (NIH).

Experimental animal models of cutaneous fibrosis

To evaluate the role of Fn^{EDA} in fibrogenesis, we studied cutaneous fibrosis induced by bleomycin or by AdTGF-β1 in Fn^{EDA}-null mice (21). Eight-week-old female Fn^{EDA}-null mice and wild-type C57BL/6J mice (The Jackson Laboratory) in parallel were given daily subcutaneous injections of bleomycin (10 mg/kg per day) or PBS for 10 days (15). In other experiments, Fn^{EDA}-null mice and wild-type mice in parallel received two subcutaneous injections of AdTGF-β1 (1×10^9 plaque-forming units) or empty vector administered 14 days apart. Mice were sacrificed at day 28, and lesional skin was harvested for analysis. Four-micrometer-thick sections of paraffin-embedded tissues were stained with hematoxylin and eosin, or Masson's trichrome for visualizing collagen. Collagen deposition in the dermis was assessed in Masson's trichrome–stained slides by quantitating blue pixels with ImageJ software. Immunofluorescence analyses were performed by incubating tissues with primary rabbit antibodies against αSMA (Sigma, 1:500), Fn^{EDA} (Abcam, 1:50), or phospho-Smad2 (Cell Signaling Technology, 1:100) followed by Alexa Fluor–labeled rabbit secondary antibodies. Nuclei were detected with DAPI. Slides were mounted, and immunofluorescence was evaluated under a Zeiss UV Meta 510 confocal microscope. Each experimental group consisted of at least five mice. Elastic fibers in the skin were visualized with Verhoeff's stain followed by Van Gieson's counterstain (71). Accumulation of elastic fibers was quantitated by determining the percentage of positive pixels (elastin stained) from five randomly selected hpf per slide with Adobe Photoshop CS5 (Adobe Systems) (71).

To investigate the preventive and therapeutic effects of pharmacological TLR4 blockade on cutaneous fibrosis in vivo, C57BL/6J mice were given daily subcutaneous injections of bleomycin (10 mg/kg) or PBS for 15 days. One group of mice was given CLI-095 (2 mg/kg) (InvivoGen) by daily intraperitoneal injections starting concurrently with PBS or bleomycin, and sacrificed on day 24, whereas in another group of mice, daily CLI-095 injections were started at day 15 and mice were sacrificed on day 28. Each experimental group consisted of five mice.

Statistical analysis

Data are presented as means ± SD. Two-tailed Student's t test or Mann-Whitney *U* test was used for comparisons between two groups, and $P < 0.05$ was considered significant. Spearman's rank correlation coefficient was used to analyze the relationship between serum Fn^{EDA} levels and clinical parameters. Comparisons among three or more groups were performed with ANOVA followed by Bonferroni correction or Sidak's multiple comparison test. Data were analyzed with GraphPad Prism (version 5 or 6; GraphPad Software).

Study approval

Animal studies were conducted in accordance with the NIH *Guide for the Care and Use of Laboratory Animals* and approved by the Institutional Animal Care and Use Committee of the Northwestern University. Studies involving human subjects were approved by the Institutional Review Board of the Northwestern University, and all the participants provided written informed consent.

Supplementary Material

Refer to Web version on PubMed Central for supplementary material.

Acknowledgments

We are grateful to R. P. Schleimer, A. Dreffs, and A. Booth for reagents, and W. Tourtellotte, S. Hussain, and members of the Varga and Shea laboratories and the staff of the Northwestern University Imaging Core for helpful discussions and excellent technical support. The Skin Diseases Research Core assisted with construction of human skin equivalents. **Funding:** Supported by grants from the National Institute of Arthritis and Musculoskeletal and Skin Diseases (AR42309 and AR057216).

REFERENCES AND NOTES

1. Denton CP, Ong VH. Targeted therapies for systemic sclerosis. Nat. Rev. Rheumatol. 2013; 9:451–464. [PubMed: 23567456]
2. Rosenbloom J, Castro SV, Jimenez SA. Narrative review: Fibrotic diseases: Cellular and molecular mechanisms and novel therapies. Ann. Intern. Med. 2010; 152:159–166. [PubMed: 20124232]
3. Varga J, Rosenbloom J, Jimenez SA. Transforming growth factor β (TGFβ) causes a persistent increase in steady-state amounts of type I and type III collagen and fibronectin mRNAs in normal human dermal fibroblasts. Biochem. J. 1987; 247:597–604. [PubMed: 3501287]
4. Varga J, Abraham D. Systemic sclerosis: A prototypic multisystem fibrotic disorder. J. Clin. Invest. 2007; 117:557–567. [PubMed: 17332883]
5. Hinz B, Phan SH, Thannickal VJ, Prunotto M, Desmoulière A, Varga J, De Wever O, Mareel M, Gabbiani G. Recent developments in myofibroblast biology: Paradigms for connective tissue remodeling. Am. J. Pathol. 2012; 180:1340–1355. [PubMed: 22387320]
6. Bhattacharyya S, Wei J, Varga J. Understanding fibrosis in systemic sclerosis: Shifting paradigms, emerging opportunities. Nat. Rev. Rheumatol. 2012; 8:42–54. [PubMed: 22025123]
7. Piccinini AM, Midwood KS. DAMPening inflammation by modulating TLR signalling. Mediators Inflamm. 2010; 2010:672395. [PubMed: 20706656]
8. Kono H, Rock KL. How dying cells alert the immune system to danger. Nat. Rev. Immunol. 2008; 8:279–289. [PubMed: 18340345]
9. Beutler B. Neo-ligands for innate immune receptors and the etiology of sterile inflammatory disease. Immunol. Rev. 2007; 220:113–128. [PubMed: 17979843]
10. Tolle LB, Standiford TJ. Danger-associated molecular patterns (DAMPs) in acute lung injury. J. Pathol. 2013; 229:145–156. [PubMed: 23097158]

11. Huebener P, Schwabe RF. Regulation of wound healing and organ fibrosis by toll-like receptors. Biochim. Biophys. Acta. 2013; 1832:1005–1017. [PubMed: 23220258]
12. Seki E, De Minicis S, Osterreicher CH, Kluwe J, Osawa Y, Brenner DA, Schwabe RF. TLR4 enhances TGF-β signaling and hepatic fibrosis. Nat. Med. 2007; 13:1324–1332. [PubMed: 17952090]
13. Pulskens WP, Rampanelli E, Teske GJ, Butter LM, Claessen N, Luirink IK, van der Poll T, Florquin S, Leemans JC. TLR4 promotes fibrosis but attenuates tubular damage in progressive renal injury. J. Am. Soc. Nephrol. 2010; 21:1299–1308. [PubMed: 20595685]
14. Campbell MT, Hile KL, Zhang H, Asanuma H, Vanderbrink BA, Rink RR, Meldrum KK. Toll-like receptor 4: A novel signaling pathway during renal fibrogenesis. J. Surg. Res. 2011; 168:e61–e69. [PubMed: 20089260]
15. Bhattacharyya S, Kelley K, Melichian DS, Tamaki Z, Fang F, Su Y, Feng G, Pope RM, Budinger GR, Mutlu GM, Lafyatis R, Radstake T, Feghali-Bostwick C, Varga J. Toll-like receptor 4 signaling augments transforming growth factor-β responses: A novel mechanism for maintaining and amplifying fibrosis in scleroderma. Am. J. Pathol. 2013; 182:192–205. [PubMed: 23141927]
16. Ciechomska M, Cant R, Finnigan J, van Laar JM, O'Reilly S. Role of toll-like receptors in systemic sclerosis. Expert Rev. Mol. Med. 2013; 15:e9. [PubMed: 23985302]
17. White ES, Baralle FE, Muro AF. New insights into form and function of fibronectin splice variants. J. Pathol. 2008; 216:1–14. [PubMed: 18680111]
18. Muro AF, Caputi M, Pariyarath R, Pagani F, Buratti E, Baralle FE. Regulation of fibronectin EDA exon alternative splicing: Possible role of RNA secondary structure for enhancer display. Mol. Cell. Biol. 1999; 19:2657–2671. [PubMed: 10082532]
19. Serini G, Bochaton-Piallat ML, Ropraz P, Geinoz A, Borsi L, Zardi L, Gabbiani G. The fibronectin domain ED-A is crucial for myofibroblastic phenotype induction by transforming growth factor-β1. J. Cell Biol. 1998; 142:873–881. [PubMed: 9700173]
20. To WS, Midwood KS. Plasma and cellular fibronectin: Distinct and independent functions during tissue repair. Fibrogenesis Tissue Repair. 2011; 4:21. [PubMed: 21923916]
21. Muro AF, Chauhan AK, Gajovic S, Iaconcig A, Porro F, Stanta G, Baralle FE. Regulated splicing of the fibronectin EDA exon is essential for proper skin wound healing and normal lifespan. J. Cell Biol. 2003; 162:149–160. [PubMed: 12847088]
22. Kuhn C, McDonald JA. The roles of the myofibroblast in idiopathic pulmonary fibrosis. Ultrastructural and immunohistochemical features of sites of active extracellular matrix synthesis. Am. J. Pathol. 1991; 138:1257–1265. [PubMed: 2024710]
23. Hernnäs J, Nettelbladt O, Bjermer L, Särnstrand B, Malmström A, Hällgren R. Alveolar accumulation of fibronectin and hyaluronan precedes bleomycin-induced pulmonary fibrosis in the rat. Eur. Respir. J. 1992; 5:404–410. [PubMed: 1373389]
24. Muro AF, Moretti FA, Moore BB, Yan M, Atrasz RG, Wilke CA, Flaherty KR, Martinez FJ, Tsui JL, Sheppard D, Baralle FE, Toews GB, White ES. An essential role for fibronectin extra type III domain A in pulmonary fibrosis. Am. J. Respir. Crit. Care Med. 2008; 177:638–645. [PubMed: 18096707]
25. Okamura Y, Watari M, Jerud ES, Young DW, Ishizaka ST, Rose J, Chow JC, Strauss JF III. The extra domain A of fibronectin activates Toll-like receptor 4. J. Biol. Chem. 2001; 276:10229–10233. [PubMed: 11150311]
26. Gondokaryono SP, Ushio H, Niyonsaba F, Hara M, Takenaka H, Jayawardana ST, Ikeda S, Okumura K, Ogawa H. The extra domain A of fibronectin stimulates murine mast cells via Toll-like receptor 4. J. Leukocyte Biol. 2007; 82:657–665. [PubMed: 17575266]
27. Sofat N, Robertson SD, Wait R. Fibronectin III 13-14 domains induce joint damage via Toll-like receptor 4 activation and synergize with interleukin-1 and tumour necrosis factor. J. Innate Immun. 2012; 4:69–79. [PubMed: 21997473]
28. Lefebvre JS, Lévesque T, Picard S, Paré G, Gravel A, Flamand L, Borgeat P. Extra domain A of fibronectin primes leukotriene biosynthesis and stimulates neutrophil migration through activation of Toll-like receptor 4. Arthritis Rheum. 2011; 63:1527–1533. [PubMed: 21360520]
29. Hubmacher D, Apte SS. The biology of the extracellular matrix: Novel insights. Curr. Opin. Rheumatol. 2013; 25:65–70. [PubMed: 23143224]

30. Turino GM, Ma S, Lin YY, Cantor JO, Luisetti M. Matrix elastin: A promising biomarker for chronic obstructive pulmonary disease. Am. J. Respir. Crit. Care Med. 2011; 184:637–641. [PubMed: 21757624]
31. Klingberg F, Hinz B, White ES. The myofibroblast matrix: Implications for tissue repair and fibrosis. J. Pathol. 2013; 229:298–309. [PubMed: 22996908]
32. Chatterjee S, Mark ME, Wooley PH, Lawrence WD, Mayes MD. Increased dermal elastic fibers in the tight skin mouse. Clin. Exp. Rheumatol. 2004; 22:617–620. [PubMed: 15485016]
33. Walters R, Pulitzer M, Kamino H. Elastic fiber pattern in scleroderma/morphea. J. Cutan. Pathol. 2009; 36:952–957. [PubMed: 19674200]
34. Lemaire R, Korn JH, Schiemann WP, Lafyatis R. Fibulin-2 and fibulin-5 alterations in Tsk mice associated with disorganized hypodermal elastic fibers and skin tethering. J. Invest. Dermatol. 2004; 123:1063–1069. [PubMed: 15610515]
35. Rhee S. Fibroblasts in three dimensional matrices: Cell migration and matrix remodeling. Exp. Mol. Med. 2009; 41:858–865. [PubMed: 19745603]
36. Wu M, Melichian DS, de la Garza M, Gruner K, Bhattacharyya S, Barr L, Nair A, Shahrara S, Sporn PH, Mustoe TA, Tourtellotte WG, Varga J. Essential roles for early growth response transcription factor Egr-1 in tissue fibrosis and wound healing. Am. J. Pathol. 2009; 175:1041–1055. [PubMed: 19679873]
37. Wells RG. The role of matrix stiffness in regulating cell behavior. Hepatology. 2008; 47:1394–1400. [PubMed: 18307210]
38. Balestrini JL, Chaudhry S, Sarrazy V, Koehler A, Hinz B. The mechanical memory of lung myofibroblasts. Integr. Biol. 2012; 4:410–421.
39. Liu F, Mih JD, Shea BS, Kho AT, Sharif AS, Tager AM, Tschumperlin DJ. Feedback amplification of fibrosis through matrix stiffening and COX-2 suppression. J. Cell Biol. 2010; 190:693–706. [PubMed: 20733059]
40. Kawamoto T, Ii M, Kitazaki T, Iizawa Y, Kimura H. TAK-242 selectively suppresses Toll-like receptor 4-signaling mediated by the intracellular domain. Eur. J. Pharmacol. 2008; 584:40–48. [PubMed: 18299127]
41. Hoshino K, Takeuchi O, Kawai T, Sanjo H, Ogawa T, Takeda Y, Takeda K, Akira S. Cutting edge: Toll-like receptor 4 (TLR4)-deficient mice are hyporesponsive to lipopolysaccharide: Evidence for TLR4 as the Lps gene product. J. Immunol. 1999; 162:3749–3752. [PubMed: 10201887]
42. Maurer B, Stanczyk J, Jüngel A, Akhmetshina A, Trenkmann M, Brock M, Kowal-Bielecka O, Gay RE, Michel BA, Distler JH, Gay S, Distler O. MicroRNA-29, a key regulator of collagen expression in systemic sclerosis. Arthritis Rheum. 2010; 62:1733–1743. [PubMed: 20201077]
43. Schulz MH, Pandit KV, Lino Cardenas CL, Ambalavanan N, Kaminski N, Bar-Joseph Z. Reconstructing dynamic microRNA-regulated interaction networks. Proc. Natl. Acad. Sci. U.S.A. 2013; 110:15686–15691. [PubMed: 23986498]
44. Rybak JN, Roesli C, Kaspar M, Villa A, Neri D. The extra-domain A of fibronectin is a vascular marker of solid tumors and metastases. Cancer Res. 2007; 67:10948–10957. [PubMed: 18006840]
45. Matsumoto E, Yoshida T, Kawarada Y, Sakakura T. Expression of fibronectin isoforms in human breast tissue: Production of extra domain A^+/extra domain B^+ by cancer cells and extra domain A^+ by stromal cells. Jpn. J. Cancer Res. 1999; 90:320–325. [PubMed: 10359047]
46. Liu H, Chen B, Zardi L, Ramos DM. Soluble fibronectin promotes migration of oral squamous-cell carcinoma cells. Int. J. Cancer. 1998; 78:261–267. [PubMed: 9754661]
47. Flanagan M, Liang H, Norton PA. Alternative splicing of fibronectin mRNAs in chondrosarcoma cells: Role of far upstream intron sequences. J. Cell. Biochem. 2003; 90:709–718. [PubMed: 14587027]
48. Kriegsmann J, Berndt A, Hansen T, Borsi L, Zardi L, Bräuer R, Petrow PK, Otto M, Kirkpatrick CJ, Gay S, Kosmehl H. Expression of fibronectin splice variants and oncofetal glycosylated fibronectin in the synovial membranes of patients with rheumatoid arthritis and osteoarthritis. Rheumatol. Int. 2004; 24:25–33. [PubMed: 12712258]
49. Claudepierre P, Allanore Y, Belec L, Larget-Piet B, Zardi L, Chevalier X. Increased Ed-B fibronectin plasma levels in spondyloarthropathies: Comparison with rheumatoid arthritis patients and a healthy population. Rheumatology. 1999; 38:1099–1103. [PubMed: 10556262]

50. Hackl NJ, Bersch C, Feick P, Antoni C, Franke A, Singer MV, Nakchbandi IA. Circulating fibronectin isoforms predict the degree of fibrosis in chronic hepatitis C. Scand. J. Gastroenterol. 2010; 45:349–356. [PubMed: 20017652]
51. Rajkumar VS, Howell K, Csiszar K, Denton CP, Black CM, Abraham DJ. Shared expression of phenotypic markers in systemic sclerosis indicates a convergence of pericytes and fibroblasts to a myofibroblast lineage in fibrosis. Arthritis Res. Ther. 2005; 7:R1113–R1123. [PubMed: 16207328]
52. Ihn H. Autocrine TGF-β signaling in the pathogenesis of systemic sclerosis. J. Dermatol. Sci. 2008; 49:103–113. [PubMed: 17628443]
53. Balza E, Borsi L, Allemanni G, Zardi L. Transforming growth factor β regulates the levels of different fibronectin isoforms in normal human cultured fibroblasts. FEBS Lett. 1988; 228:42–44. [PubMed: 3422628]
54. White ES, Sagana RL, Booth AJ, Yan M, Cornett AM, Bloomheart CA, Tsui JL, Wilke CA, Moore BB, Ritzenthaler JD, Roman J, Muro AF. Control of fibroblast fibronectin expression and alternative splicing via the PI3K/Akt/mTOR pathway. Exp. Cell Res. 2010; 316:2644–2653. [PubMed: 20615404]
55. Arslan F, Smeets MB, Riem Vis PW, Karper JC, Quax PH, Bongartz LG, Peters JH, Hoefer IE, Doevendans PA, Pasterkamp G, de Kleijn DP. Lack of fibronectin-EDA promotes survival and prevents adverse remodeling and heart function deterioration after myocardial infarction. Circ. Res. 2011; 108:582–592. [PubMed: 21350212]
56. Shinde AV, Bystroff C, Wang C, Vogelezang MG, Vincent PA, Hynes RO, Van De Water L. Identification of the peptide sequences within the EIIIA (EDA) segment of fibronectin that mediate integrin α9β1-dependent cellular activities. J. Biol. Chem. 2008; 283:2858–2870. [PubMed: 17967897]
57. Liao YF, Gotwals PJ, Koteliansky VE, Sheppard D, Van De Water L. The EIIIA segment of fibronectin is a ligand for integrins α9β1 and α4β1 providing a novel mechanism for regulating cell adhesion by alternative splicing. J. Biol. Chem. 2002; 277:14467–14474. [PubMed: 11839764]
58. Thannickal VJ, Lee DY, White ES, Cui Z, Larios JM, Chacon R, Horowitz JC, Day RM, Thomas PE. Myofibroblast differentiation by transforming growth factor-β1 is dependent on cell adhesion and integrin signaling via focal adhesion kinase. J. Biol. Chem. 2003; 278:12384–12389. [PubMed: 12531888]
59. Fernandes DJ, Bonacci JV, Stewart AG. Extracellular matrix, integrins, and mesenchymal cell function in the airways. Curr. Drug Targets. 2006; 7:567–577. [PubMed: 16719767]
60. Khan MM, Gandhi C, Chauhan N, Stevens JW, Motto DG, Lentz SR, Chauhan AK. Alternatively-spliced extra domain A of fibronectin promotes acute inflammation and brain injury after cerebral ischemia in mice. Stroke. 2012; 43:1376–1382. [PubMed: 22363055]
61. Kogure T, Costinean S, Yan I, Braconi C, Croce C, Patel T. Hepatic miR-29ab1 expression modulates chronic hepatic injury. J. Cell. Mol. Med. 2012; 16:2647–2654. [PubMed: 22469499]
62. Zhong X, Chung AC, Chen HY, Meng XM, Lan HY. Smad3-mediated upregulation of miR-21 promotes renal fibrosis. J. Am. Soc. Nephrol. 2011; 22:1668–1681. [PubMed: 21852586]
63. Roderburg C, Urban GW, Bettermann K, Vucur M, Zimmermann H, Schmidt S, Janssen J, Koppe C, Knolle P, Castoldi M, Tacke F, Trautwein C, Luedde T. Micro-RNA profiling reveals a role for miR-29 in human and murine liver fibrosis. Hepatology. 2011; 53:209–218. [PubMed: 20890893]
64. Pandit KV, Milosevic J, Kaminski N. MicroRNAs in idiopathic pulmonary fibrosis. Transl. Res. 2011; 157:191–199. [PubMed: 21420029]
65. Yang T, Liang Y, Lin Q, Liu J, Luo F, Li X, Zhou H, Zhuang S, Zhang H. MiR-29 mediates TGFβ1-induced extracellular matrix synthesis through activation of PI3K-AKT pathway in human lung fibroblasts. J. Cell Biochem. 2013; 114:1336–1342. [PubMed: 23238947]
66. Preliminary criteria for the classification of systemic sclerosis (scleroderma). Subcommittee for scleroderma criteria of the American Rheumatism Association Diagnostic and Therapeutic Criteria Committee. Arthritis Rheum. 1980; 23:581–590. [PubMed: 7378088]

67. LeRoy EC, Black C, Fleischmajer R, Jablonska S, Krieg T, Medsger TA Jr. Rowell N, Wollheim F. Scleroderma (systemic sclerosis): Classification, subsets and pathogenesis. J. Rheumatol. 1988; 15:202–205. [PubMed: 3361530]

68. Hinchcliff M, Huang CC, Wood TA, Mahoney JM, Martyanov V, Bhattacharyya S, Tamaki Z, Carns M, Podlusky S, Sirajuddin A, Shah SJ, Lee J, Chang RW, Lafyatis R, Varga J, Whitfield ML. Molecular signatures in skin associated with clinical improvement during mycophenolate treatment in systemic sclerosis. J. Invest. Dermatol. 2013; 133:1979–1989. [PubMed: 23677167]

69. Getsios S, Simpson CL, Kojima S, Harmon R, Sheu LJ, Dusek RL, Cornwell M, Green KJ. Desmoglein 1–dependent suppression of EGFR signaling promotes epidermal differentiation and morphogenesis. J. Cell Biol. 2009; 185:1243–1258. [PubMed: 19546243]

70. Simpson CL, Kojima S, Getsios S. RNA interference in keratinocytes and an organotypic model of human epidermis. Methods Mol. Biol. 2010; 585:127–146. [PubMed: 19908001]

71. Pellicoro A, Aucott RL, Ramachandran P, Robson AJ, Fallowfield JA, Snowdon VK, Hartland SN, Vernon M, Duffield JS, Benyon RC, Forbes SJ, Iredale JP. Elastin accumulation is regulated at the level of degradation by macrophage metalloelastase (MMP-12) during experimental liver fibrosis. Hepatology. 2012; 55:1965–1975. [PubMed: 22223197]

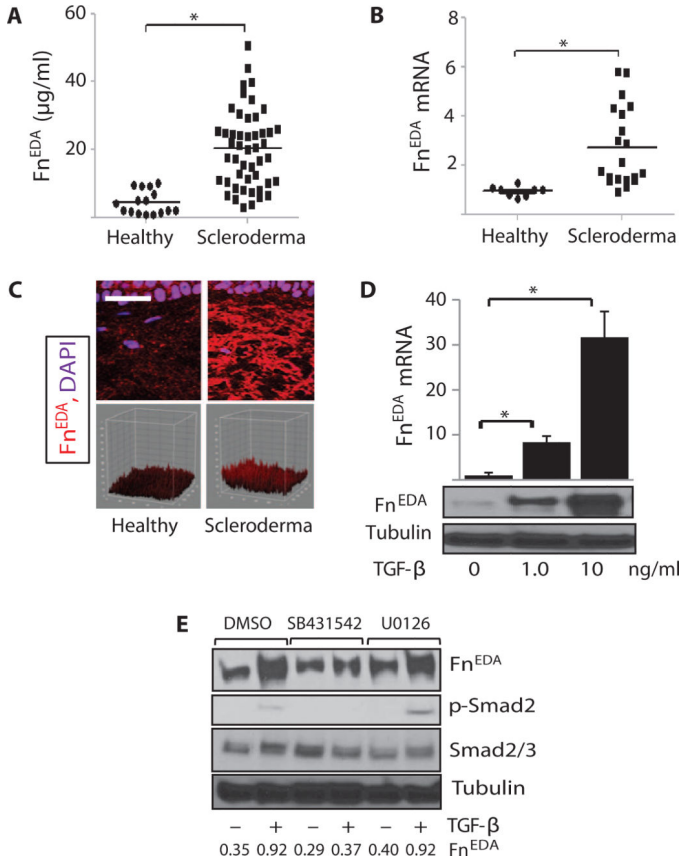

Fig. 1. Fn^{EDA} is elevated in scleroderma, and its expression is stimulated by TGF-β

(**A**) Fn^{EDA} serum levels in scleroderma patients (n = 48) and healthy adults (n = 16) were determined by enzyme-linked immunosorbent assay (ELISA). Each data point is the mean ± SD of trip-licate determinations from a single subject. *P < 0.0001, Mann-Whitney U test. (**B**) RNA isolated from skin biopsies from scleroderma patients (n = 20) and healthy adults (n = 8) was analyzed by real-time qPCR. Results, expressed relative to glyceraldehyde-3-phosphate dehydrogenase (GAPDH), are the means ± SD of duplicate determinations. *P = 0.0002, Mann-Whitney U test. (**C**) Immunofluorescence analysis. Skin biopsies from scleroderma patients (n = 13) and healthy controls (n = 6) in parallel were immunostained with antibodies to Fn^{EDA} and examined by immunofluorescence confocal microscopy. Upper panels: Representative images. Scale bar, 25 μm. Lower panels: 3D plots of fluorescence intensity (see Table 3). P = 0.0159, Mann-Whitney U test. (**D** and **E**) Confluent human skin fibroblasts were incubated for 24 hours with TGF-β (1 and 10 ng/ml) alone (D) or in the presence or absence of SB431542 or U0126 (E). (D) Upper panel: Levels of mRNA were determined by real-time quantitative PCR. Results, normalized with GAPDH, are means ± SD of triplicate determinations. *P < 0.0001, one-way analysis of variance (ANOVA) followed by Bonferroni's multiple comparison test. Lower panel: Whole-cell lysates were subjected to Western analysis. Representative immunoblots.

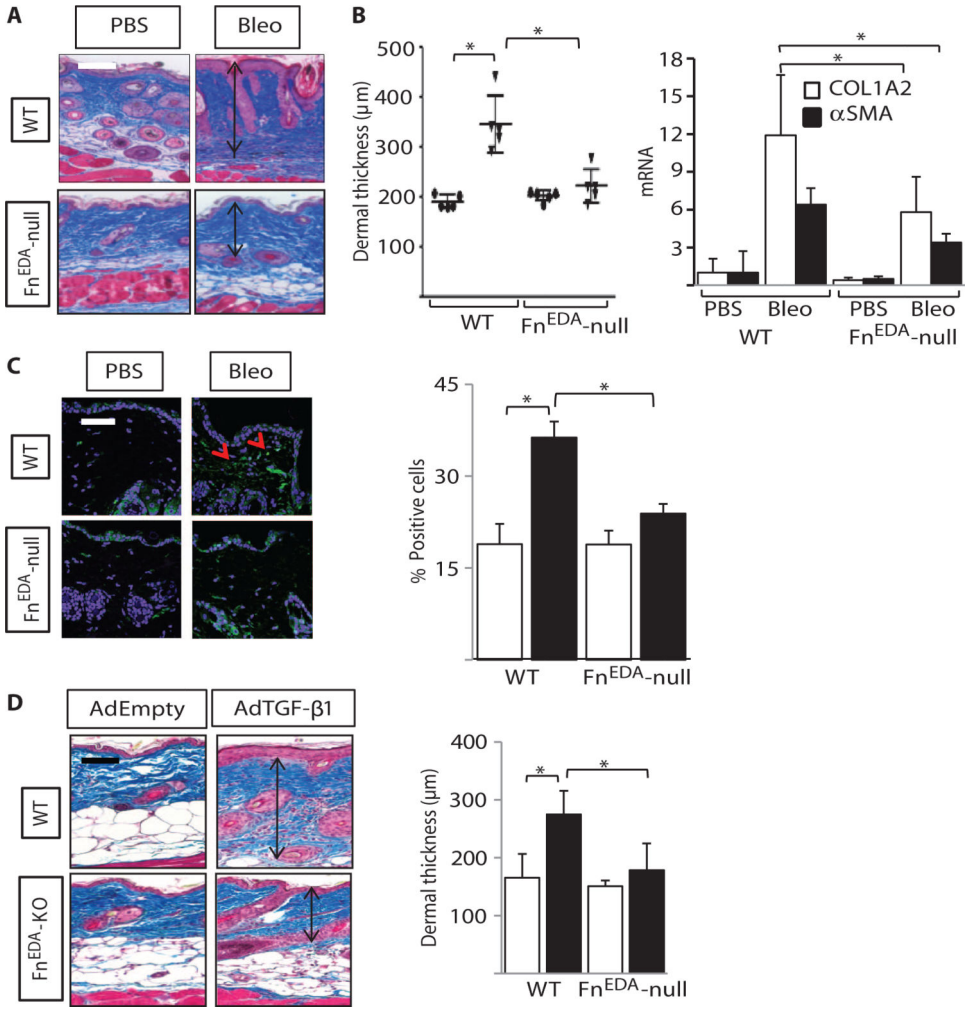

Fig. 2. Skin fibrosis is attenuated in mice lacking Fn^{EDA}

Fn^{EDA}-null mice and wild-type (WT) mice in parallel received daily subcutaneous injections of phosphate-buffered saline (PBS) or bleomycin (Bleo) for 14 days and sacrificed at day 24 (A to C), or two subcutaneous injections of AdTGF-β1 or empty vector 14 days apart and sacrificed at 28 days (D). Lesional skin was harvested for analysis. (**A**) Left panel: Masson's trichrome stain. Representative images. Arrows indicate dermis. Scale bar, 100 μm. Right panel: Dermal thickness (distance from dermal-epidermal junction to adipose layer), shown as the means ± SD of triplicate determinations per hpf from five mice per group. Ovals, PBS; inverted triangles, bleomycin. *P < 0.0001, PBS versus bleomycin; P < 0.001, WT versus Fn^{EDA}-null bleomycin, one-way ANOVA followed by Bonferroni's multiple comparison test. (**B**) mRNA levels were determined by real-time quantitative PCR. The results, normalized with GAPDH, represent the means ± SD of triplicate determinations from four mice per group. *P = 0.014, Mann-Whitney U test. (**C**) Immunofluorescence using antibodies against αSMA (green) and 4′,6′-diamidino-2-phenylindole (DAPI) (blue). Left panel: Representative images. Scale bar, 50 μm. Red arrows indicate αSMA-positive cells in the dermis. Right panel: The proportion of αSMA-immunopositive cells in the lesional dermis was determined in five randomly selected hpf per slide from four mice per

group. Open bars, PBS; closed bars, bleomycin. PBS versus bleomycin. **P* < 0.0001, WT bleomycin versus null bleomycin; *P* < 0.001, one-way ANOVA followed by Bonferroni's multiple comparison test. (**D**) Masson's trichrome stain. Left panel: Representative images. Scale bar, 100 μm. Right panel: Dermal thickness, shown as the means ± SD of triplicate determinations per hpf from four mice per group. Open bars, PBS; closed bars, AdTGF-β1. **P* = 0.02, PBS versus bleomycin; *P* = 0.03, WT versus Fn^{EDA}-null bleomycin, Sidak's multiple comparison test.

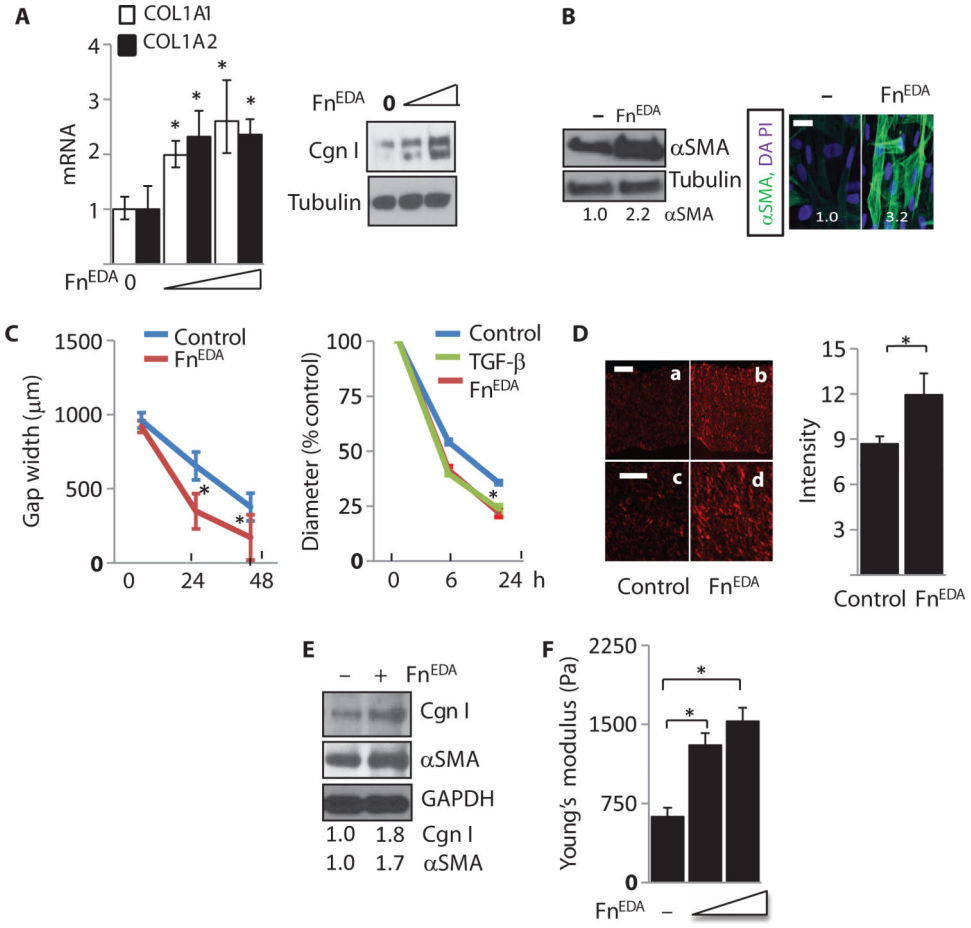

Fig. 3. Fn^{EDA} elicits profibrotic responses in normal fibroblasts

(**A** to **C**) Normal skin fibroblasts were incubated in medium with Fn^{EDA} (5 and 10 μg/ml) for 72 hours. (A) Left panel: mRNA levels were determined by real-time qPCR. Results, normalized with GAPDH, are the means ± SD of triplicate determinations from three independent experiments ($P < 0.01$, one-way ANOVA followed by Bonferroni's multiple comparison test). Open bars, COL1A1; closed bars, αSMA. Right panel: Whole-cell lysates were examined by Western analysis. Representative immunoblots. Cgn I, type I collagen. (B) Left panel: Representative immunoblots. Values below indicate fold induction (means from three independent experiments corrected for tubulin in each lane). Right panel: Slides were immunostained with antibodies to αSMA (green). Nuclei are identified by DAPI (blue). Representative images. Scale bar, 50 μm. Values indicate fold induction (means from three independent experiments). (**C**) Left panel: Fibroblasts were seeded on plates coated with Fn^{EDA} or left untreated, and at confluence, scratch wounds were created. Fibroblast migration was determined by measuring gap width at 24 and 48 hours. Results are means ± SD of triplicate determinations at three randomly selected locations from triplicate determinations (at 24 hours, $P = 0.0043$; at 48 hours, $P = 0.0450$, Mann-Whitney U test). Right panel: Collagen gel contraction assays. Fibroblasts were seeded in type I collagen gels and were incubated in medium in the presence or absence of TGF-β and Fn^{EDA} (10 μg/ml). At 6 and 24 hours, gel diameters were determined. Results, expressed as percentage of gel area compared to controls (time 0), are the means ± SD of triplicate determinations (at 24

hours: control versus TGF-β, $P < 0.0001$; control versus Fn^{EDA}, $P < 0.0001$, one-way ANOVA followed by Bonferroni's multiple comparison test). (**D**) 3D human skin equivalents constructed without or with Fn^{EDA} (10 μg/ml) were seeded with fibroblasts. After 18 days, rafts were stained with Picrosirius Red. Left panel: Representative images. Scale bars, 25 μm (a and b) or 10 μm (c and d). Right panel: Immunofluorescence intensity. Bars represent the means ± SD from six randomly selected hpf per raft from three independent raft experiments ($P = 0.022$, Mann-Whitney *U* test). (**E**) Total protein from dermal compartments was analyzed. Representative Western blot. Numbers below indicate relative band intensities (means from two independent experiments corrected for GAPDH in each lane). (**F**) Stiffness of the dermal compartment was determined as described in Materials and Methods. The results represent the means ± SD from three independent rafts ($P < 0.0001$, control versus Fn^{EDA} low; $P < 0.0001$, control versus Fn^{EDA} high, oneway ANOVA followed by Bonferroni's multiple comparison test).

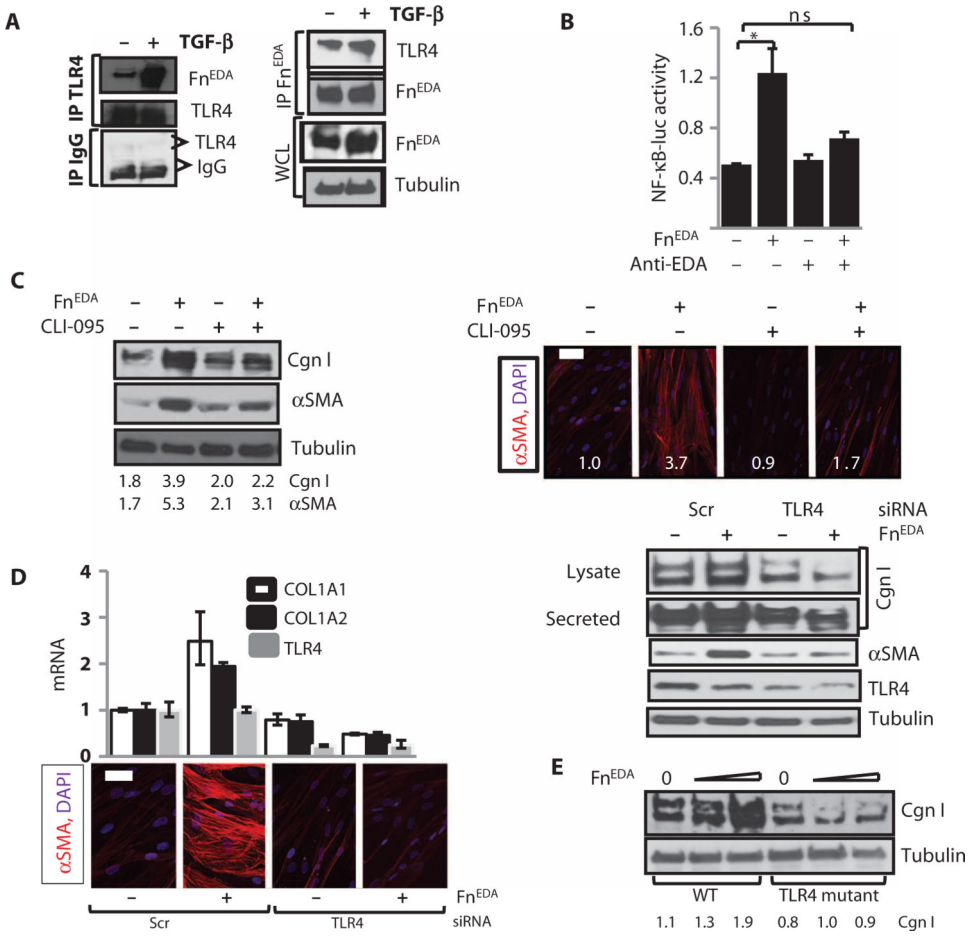

Fig. 4. Fn^{EDA} elicits TLR4-dependent fibroblast responses

(**A**) Fn^{EDA} interacts directly with TLR4. Whole-cell lysates (WCL) from normal skin fibroblasts incubated in the presence or absence of TGF-β for 24 hours were immunoprecipitated (IP) with antibodies against TLR4 or Fn^{EDA} or IgG and immunoblotted using antibodies to Fn^{EDA} or TLR4. Representative immunoblots. (**B**) Fibroblasts transiently transfected with NF-κB-luc were incubated in medium with endotoxin-stripped Fn^{EDA} in the presence or absence of neutralizing antibodies to Fn^{EDA} (anti-EDA) for 24 hours. Whole-cell lysates were assayed for their luciferase activities. Results are means ± SD from three independent experiments. *P = 0.002, control versus Fn^{EDA}; *P = 0.04, Fn^{EDA} versus anti-EDA–treated, Sidak's multiple comparison test. ns, not significant. (**C** to **E**) Human skin fibroblasts (C and D) or skin fibroblasts (E) from TLR4-mutant and WT mouse were incubated in medium with Fn^{EDA} (10 μg/ml) in the presence or absence of CLI-095 for 72 hours. (C) Left panels: Whole-cell lysates were subjected to Western analysis. Numbers below indicate relative band intensities corrected for tubulin (means from three independent experiments). Right panels: Fibroblasts were immunostained with antibodies to αSMA. Representative immunofluorescence confocal images. Scale bar, 50 μm. Numbers represent fluorescence intensity determined in four randomly selected locations per hpf for each sample (means from three independent experiments). (D) Human skin fibroblasts were transfected with TLR4-specific siRNA or scrambled (Scr) siRNA,

followed by incubation in medium with Fn^{EDA} for 72 hours. Left upper panels: mRNA levels were determined by real-time qPCR. Results, normalized with GAPDH mRNA, are means ± SD of triplicate determinations from an experiment representative of two independent experiments. Left lower panels: Immunofluorescence using antibodies to αSMA (red). Representative images. Scale bar, 50 μm. Right panels: Whole-cell lysates were examined by Western analysis. Representative immunoblots. (E) Skin fibroblasts from WT and TLR4-mutant mice in parallel were incubated in medium with Fn^{EDA} for 72 hours. Whole-cell lysates were examined by Western analysis. Representative immunoblots. Numbers below indicate relative band intensities corrected for tubulin (means from two independent experiments).

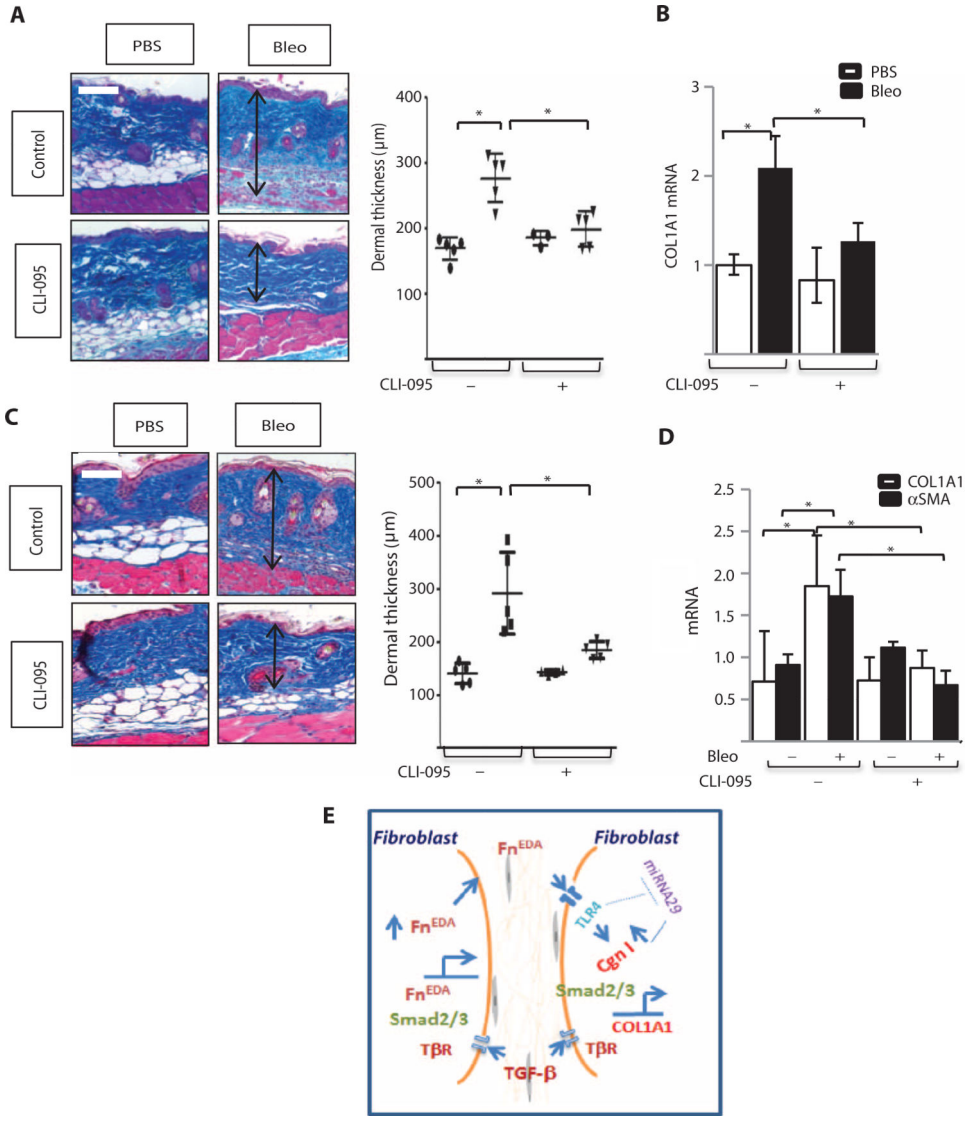

Fig. 5. Pharmacological TLR4 blockade both prevents and reverses bleomycin-induced skin fibrosis

(**A** to **D**) C57BL/6J mice received daily subcutaneous injections of bleomycin or PBS. Mice also received CLI-095 (2 mg/kg) starting on day 0 (A and B) or on day 15 (C and D) and sacrificed at day 24 (A and B) or day 28 (C and D), and lesional skin was harvested for analysis. (A and C) Masson's trichrome stain. Representative images (left panels). Scale bars, 100 μm. Right panel: Dermal thickness, determined in four random locations per hpf, is shown as means ± SD from five mice per group. Ovals, PBS; inverted triangles, bleomycin. **P* < 0.0001, PBS versus bleomycin; **P* < 0.001, bleomycin versus CLI-095, one-way ANOVA followed by Bonferroni's multiple comparison test for (A). **P* = 0.0005, PBS versus bleomycin; **P* = 0.007, bleomycin versus CLI-095, Sidak's multiple comparison test for (C). (B and D) Levels of mRNA were determined by real-time qPCR. The results, normalized for GAPDH, represent the means ± SD of triplicate determinations from four (A and B) or five (C and D) mice per group. **P* = 0.002, WT versus bleomycin; **P* = 0.014, bleomycin versus bleomycin + CLI-095, one-way ANOVA followed by Bonferroni's

multiple comparison test. (**E**) Cartoon depicting contribution of TLR4-mediated fibroblast activation elicited by Fn^{EDA} to persistent fibrogenesis. By triggering fibroblast TLR4 signaling, Fn^{EDA} serves as a switch converting self-limited tissue repair into sustained fibrogenesis. Persistent injury leads to fibroblast activation with generation and extracellular accumulation of Fn^{EDA} that in turn triggers TLR4-dependent cellular signaling, resulting in sustained fibroblast activation with production of Fn^{EDA} and other ECM molecules. A self-amplifying vicious cycle of fibrogenesis ensues.

Table 1

Subjects for serum determination of Fn^{EDA}. The serum creatinine level was 0.74 ± 0.2mg/dl (mean±SD), and only 3 of 48 patients had serum creatinine level >1.0 mg/dl; none had levels >1.35 mg/dl. Controls were healthy women (median age, 49 years; range, 34 to 62 years). dcSSc diffuse cutaneous SSc DLco, diffusing capacity for carbon monoxide; F, female; FVC, forced vital capacity; lcSSc limited cutaneous SSc; M, male; mRSS, modified Rodnan skin score (1 to 51).

Study code	Age (years)	Sex	Disease subtype	Disease stage (early/late)*	mRSS	FVC (% predicted)	DLco (% predicted)
SScReg_1010_2	57	F	dcSSc	Late	15	99	74
SScReg_1024_2	54	F	dcSSc	Late	22	67	86
SScReg_1073_2	61	F	dcSSc	Late	9	73	60
SScReg_1080_2	55	F	dcSSc	Early	19	81	82
SScReg_1084_2	57	M	dcSSc	Late	10	80	72
SScReg_1100_2	39	F	dcSSc	Early	14	61	43
SScReg_1107_2	48	M	dcSSc	Early	25	96	94
SScReg_1121_2	47	F	dcSSc	Late	26	71	75
SScReg_1046_2	37	F	dcSSc	Late	21	73	62
SScReg_1154_2	56	F	dcSSc	Late	13	87	85
SScReg_1156_2	48	F	dcSSc	Early	23	77	
SScReg_1141_2	52	F	dcSSc	Early	16	75	53
SScReg_1182_2	50	F	dcSSc	Late	9	77	61
SScReg_1213_3	30	F	dcSSc	Late	10	81	82
SScReg_1266_3	66	F	dcSSc	Early	14	64	72
SScReg_1068_2	49	F	dcSSc	Late	27	83	88
SScReg_1097_2	64	F	dcSSc	Early	9	66	65
SScReg_1103_2	54	F	dcSSc	Late	13	70	70
SScReg_1043_2	61	F	dcSSc	Late	7	78	72
SScReg_1095_2	42	F	dcSSc	Late	11	83	60
SScReg_1102_3	29	F	dcSSc	Late	20	72	56
SScReg_1048_3	39	M	dcSSc	Late	12	89	81
SScReg_1117_3	45	F	dcSSc	Late	23	94	65
SScReg_1221_3	57	F	dcSSc	Early	12	95	81
SScReg_1248_2	63	F	dcSSc	Late	36	97	64
SScReg_1258_1	57	F	dcSSc	Late	2	90	55
SScReg_1271_2	50	F	dcSSc	Late	25	56	43
SScReg_1279_3	59	F	dcSSc	Late	12	75	60
SScReg_1313_3	62	F	dcSSc	Late	49	86	44
SScReg_1332_2	47	F	dcSSc	Late	26	50	21
SScReg_1354_3	42	F	dcSSc	Early	29	100	76
SScReg_1370_2	45	F	dcSSc	Early	23	100	71
SScReg_1380_2	56	F	dcSSc	Early	7	91	42
SScReg_1386_2	63	F	dcSSc	Early	22	102	53
SScReg_1366_2	55	F	dcSSc	Early	23	76	75

Study code	Age (years)	Sex	Disease subtype	Disease stage (early/late)*	mRSS	FVC (% predicted)	DLco (% predicted)
SScReg_1392_3	47	F	dcSSc	Early	19	67	76
SScReg_1397_3	52	F	dcSSc	Late	22	105	64
SScReg_1402_3	48	F	dcSSc	Early	7	72	21
SScReg_1405_3	52	F	dcSSc	Early	13	77	58
SScReg_1410_3	56	F	dcSSc	Early	17	81	77
SScReg_1006_3	47	F	dcSSc	Late	3	101	99
SScReg_1412_3	65	F	dcSSc	Late	6	100	96
SScReg_1119_3	56	M	dcSSc	Late	38	41	26
SScReg_1198_3	59	F	dcSSc	Late	5	76	53
SScReg_1393_3	41	F	dcSSc	Late	14	40	42
SScReg_1320_3	31	F	dcSSc	Late	10	44	60
SScReg_1070_3	62	F	dcSSc	Late	13	25	15
SScReg_1426_2	28	F	dcSSc	Late	18	89	82

*Early, <2 years from first non-Raynaud disease manifestation; late, >2 years from first non-Raynaud manifestation.

Table 2

Subjects providing skin biopsies for mRNA analysis. None of the subjects had renal failure. Controls were healthy subjects (median age, 37 years; range, 30 to 63 years); 70% of the patients are female. PM, polymyositis overlap; EMS, eosinophilia-myaglia syndrome.

Study code	Age (years)	Sex	Disease subtype	Disease stage*	mRSS
S1001	52	F	dcSSc	Late	24
SSc01LA	48	F	dcSSc	Early	21
SSc01BLA	46	F	dcSSc	Early	3
SSc02BLA	41	F	dcSSc	Early	21
SSc03LA	55	F	lcSSc	Early	11
SSc04LA	60	F	lcSSc	Late	4
SSc05RA	66	F	dcSSc	Early	9
SSc06BRA	53	F	dcSSc	Early	13
SSc07BLA	52	F	dcSSc	Early	17
SSc08BLA	34	F	dcSSc	Late	32
SSc10BLA	27	F	dcSSc	Late	26
SSc12 BLA	21	M	dcSSc	Early	15
SSc1002BLA	56	F	dcSSc	Late	34
SSc1004BLA	55	F	dcSSc	Early	19
SSc1066LA	26	F	lcSSc	Late	5
SSc1067LA	54	F	dcSSc	Late	13
SSc1080LA	48	F	SSc/PM	Early	20
SSc1096LA	45	F	EMS	Early	23
SSc1103BLA	30	F	dcSSc	Late	4
SSc1156BLA	50	F	dcSSc	Early	14

*Early, <2 years from first non-Raynaud disease manifestation;late, >2 years from first non-Raynaud manifestation.

Table 3

Subjects providing skin biopsies for immunofluorescence analysis. None of the subjects had renal failure. Controls were healthy subjects (median age, 54 years; range, 45 to 63 years); 95% of the patients are female.

Study code	Age (years)	Sex	SSc type	Early/late (<2 years for early)*	mRSS	Fn^{EDA}†
SScMH_03_Base_LA	48	F	dcSSc	Early	21	10.59
SScMH_04_Base_LA	45	F	dcSSc	Early	9	24.20
SScMH_05_Base_RA	40	F	dcSSc	Early	32	5.64
SScMH_06_Base_RA	54	F	lcSSc	Early	16	15.00
SScMH_08_Base_LA	65	F	dcSSc	Early	12	17.55
SScMH_12_Base_LA	51	F	dcSSc	Early	14	7.52
SScMH_13_Base_LA	57	F	dcSSc	Early	17	17.03
SScMH_15_Base_LA	63	F	dcSSc	Late	36	39.26
SScMH_17_Base_LA	53	M	dcSSc	Early	35	16.26
SScMH_18_Base_LA	57	F	dcSSc	Late	11	16.92
SScMH_20_Base_LA	59	F	dcSSc	Late	12	12.84
SScMH_27_Base_LA	47	F	dcSSc	Early	29	29.07
SScMH_31_Base_LA	56	F	dcSSc	Early	15	18.82

*Early, <2 years from first non-Raynaud disease manifestation; late, >2 years from first non-Raynaud manifestation.

†Immunofluorescence intensity. Each data point represents the mean intensity from four randomly selected high-power fields (hpfs) per sample. Mean immunofluorescence intensity in healthy control biopsies ($n = 6$) was 7.86 ± 4.62. $P < 0.016$ (healthy versus SSc) (Mann-Whitney U test).